


# Reduction of elevated *Gli3* does not alter the progression of autosomal recessive polycystic kidney disease

Lauren G. Russell<sup>1,2</sup> | Maria Kolatsi-Joannou<sup>1,2</sup> | Laura Wilson<sup>1,2</sup> |  
 Jennifer C. Chandler<sup>1,2</sup> | Nuria Perretta Tejedor<sup>1,2</sup> | Georgie Stagg<sup>1,2</sup> |  
 Karen L. Price<sup>1,2</sup> | Christopher J. Rowan<sup>3</sup> | Tessa Crompton<sup>4</sup> |  
 Norman D. Rosenblum<sup>3</sup> | Paul J. D. Winyard<sup>1,2</sup> | David A. Long<sup>1,2</sup> 

<sup>1</sup>Developmental Biology and Cancer Research and Teaching Department, University College London, Great Ormond Street Institute of Child Health, London, UK

<sup>2</sup>UCL Centre for Kidney and Bladder Health, University College London, London, UK

<sup>3</sup>Department of Paediatrics, Program in Developmental and Stem Cell Biology, Hospital for Sick Children, University of Toronto, Toronto, Ontario, Canada

<sup>4</sup>Infection, Immunity and Inflammation Research and Teaching Department, University College London, Great Ormond Street Institute of Child Health, London, UK

## Correspondence

David A. Long, Kidney Development and Disease Group, Developmental Biology and Cancer Research and Teaching Department, University College London, Great Ormond Street Institute of Child Health, London, WC1N 1EH, UK.  
 Email: [d.long@ucl.ac.uk](mailto:d.long@ucl.ac.uk)

## Funding information

Kidney Research UK, Grant/Award Number: ST\_006\_20181123; University College London Research Culture Award; Wellcome Trust (WT), Grant/Award Number: 220895/Z/20/Z; UKRI | Biotechnology and Biological Sciences Research Council (BBSRC), Grant/Award Number: BB/X512011/1; NIHR | NIHR Great Ormond Street Hospital Biomedical Research Centre (BRC); Gouvernement du Canada | Canadian Institutes of Health Research (IRSC)

## Abstract

Polycystic kidney diseases (PKD) are genetic disorders which disrupt kidney architecture and function. Autosomal recessive PKD (ARPKD) is a rare form of PKD, caused by mutations in *PKHD1*, and clinically more severe than the more common autosomal dominant PKD (ADPKD). Prior studies have implicated Hedgehog (Hh) signaling in ADPKD, with increased levels of Hh components in experimental ADPKD and reduced cystogenesis following pharmacological Hh inhibition. In contrast, the role of the Hh pathway in ARPKD is poorly understood. We hypothesized that Hh pathway activity would be elevated during ARPKD pathogenesis, and its modulation may slow disease progression. We utilized *Cpk* mice which phenocopy ARPKD and generated a *PKHD1*-mutant spheroid model in human collecting ducts. Significantly elevated levels of the Hh transcriptional effector *Gli3* were found in *Cpk* mice, a finding replicated in *PKHD1*-mutant spheroids. In *Cpk* mice, total GLI3 and GLI3 repressor protein levels were also increased. Reduction of increased *Gli3* levels via heterozygous genetic deletion in *Cpk* mice did not affect cyst formation. Additionally, lowering *GLI3* transcripts to wildtype levels did not influence *PKHD1*-mutant spheroid size. Collectively, these data suggest attenuation of elevated *Gli3* does not modulate murine and human models of ARPKD.

This is an open access article under the terms of the [Creative Commons Attribution](https://creativecommons.org/licenses/by/4.0/) License, which permits use, distribution and reproduction in any medium, provided the original work is properly cited.

© 2025 The Author(s). *Physiological Reports* published by Wiley Periodicals LLC on behalf of The Physiological Society and the American Physiological Society.

## KEYWORDS

autosomal recessive polycystic kidney disease, cystogenesis, hedgehog signaling, human model, mouse model

## 1 | INTRODUCTION

Polycystic kidney disease (PKD) is characterized by the formation of fluid-filled renal cysts, which disrupt the architecture and function of the kidney and is the most common genetic cause of end stage kidney disease (ESKD). The two main forms of PKD are autosomal dominant PKD (ADPKD) and autosomal recessive PKD (ARPKD) which are caused by mutations in *PKD1* or *PKD2* (encoding polycystin-1 and -2) and *PKHD1* (encoding for fibrocystin), respectively (Bergmann et al., 2018). ARPKD has a prevalence of 1:20,000, usually manifesting in utero, perinatally or during childhood, and presenting with enlarged cystic kidneys. In ARPKD, early proximal tubular dilation is observed in the kidney during fetal development, which then shifts to dilation and cyst formation in the distal tubules and predominantly the collecting duct (Nakanishi et al., 2000). Disease progression occurs rapidly leading to the presence of cysts throughout the kidney destroying the normal renal architecture, along with interstitial fibrosis (Bergmann et al., 2018). Patients with ARPKD frequently progress to ESKD and require renal replacement therapy. Currently the only approved treatment for adults with ADPKD is tolvaptan, a vasopressin receptor 2 antagonist targeting cAMP signaling. While there are two ongoing phase 3 trials for tolvaptan in infants and children, it is not yet approved for children with PKD and there are no other treatment options for ARPKD patients (Mekahli et al., 2023). Thus, there is a need for a greater understanding of the mechanisms of disease in ARPKD to aid the development of novel treatments.

The disease-causing genes mutated in PKD patients localize to the primary cilia. This has led to an interest in the ciliary-located Hedgehog (Hh) pathway as a possible mediator in the pathogenesis of PKD (Clearman et al., 2023). Hh signaling is activated through the binding of Hh ligands to the transmembrane receptor, Patched1 (PTCH1). In the absence of Hh ligands, smoothed (SMO), a G protein-coupled receptor, is constitutively inhibited by PTCH1. This prevents the translocation of SMO to the primary cilium which allows for the phosphorylation of the GLI transcription factors (GLI1, GLI2, and GLI3). Phosphorylated GLI proteins are partially degraded by the proteasome to form a truncated repressive form of GLI, which translocates to the nucleus and represses the transcription of Hh target genes (Briscoe & Therond, 2013). When Hh ligands bind to PTCH1, the constitutive repression of SMO is blocked, leading to its translocation and accumulation in the primary cilium. GLI

transcription factors are then transported to the ciliary tip in a complex with suppressor of fused (SUFU). Full-length GLI proteins dissociate from this complex and translocate to the nucleus to activate the transcription of genes, such as those that regulate the cell cycle, proliferation, and apoptosis (Bangs & Anderson, 2017; Briscoe & Therond, 2013).

Components of the Hh signaling pathway are elevated in human ADPKD tissue (Silva et al., 2018; Song et al., 2009), mice with mutations in the ciliary genes, *Ift140*, *Thm1*, and *Arl13b* (Jonassen et al., 2012; Li et al., 2016; Tran et al., 2014); two ADPKD models, the *jck* mutant and the conditional deletion of *Pkd1* in postnatal mice (Tran et al., 2014); as well as in cystic murine metanephric kidney explants (Chan et al., 2010). Modulation of the Hh pathway through pharmacological inhibition has been demonstrated to be effective in reducing cyst progression in in vitro (Chan et al., 2010; Silva et al., 2018) and mouse models (Hsieh et al., 2022; Sato et al., 2018). The *Pck* ARPKD rat model also shows elevated SMO and GLI proteins in the lining of the cyst epithelium and responded to treatment with the SMO inhibitor, cyclopamine, leading to reduced renal cyst area (Sato et al., 2018). Furthermore, treatment with GANT61, a GLI1/2 inhibitor, alleviated the cystic phenotype and interstitial fibrosis in a ciliary mutant mouse (Hsieh et al., 2022; Li et al., 2016). Conversely, in a *Pkd1*-mutant mouse, the genetic overactivation or deletion of *Smo*, or deletion of both *Gli2* and *Gli3*, specifically in renal epithelial cells did not alter cyst formation. This study suggested that Hh signaling is not critical within the tubule epithelium in mediating cystogenesis caused by mutations in *Pkd1* (Ma et al., 2019). Thus, the function of Hh signaling in various PKD models is complex and remains only partially deciphered. In the context of ARPKD, Hh signaling has only been investigated in the *Pck* rat model (Sato et al., 2018), with no prior studies examining the pathway in either in vitro or mouse models.

In this study, we examined the role of Hedgehog signaling in murine and human models of ARPKD. We utilized the *Cpk* mouse, which contains a deletion in the ciliary gene, cystin (*Cys1*), and rapidly develops cystic kidneys, phenocopying the pathology of human ARPKD (Hou et al., 2002). We observed significant upregulation of the downstream Hh pathway effector *Gli3* in both *Cpk*<sup>-/-</sup> mice and *PKHD1*-mutant human collecting duct cells. We then reversed the increased levels of *Gli3* in both models and saw no effect on disease progression in vivo or spheroid size in vitro. These results suggest that although *Gli3* is upregulated in ARPKD models, its modulation does not alter disease progression.

## 2 | METHODS

### 2.1 | Experimental animal and procedures

All animal procedures were approved by the UK Home Office (PPL: PE52D8C09 and PP1776587) and were compliant with the UK Animals (Scientific Procedures) Act 1986. *Cpk*<sup>+/-</sup> mice (Mandell et al., 1983) were bred to generate wildtype and homozygous littermates for analysis. To decrease *Gli3* levels, heterozygous *Gli3*<sup>X<sup>tl</sup>/</sup> mice (Hui & Joyner, 1993) were crossed with *Cpk* heterozygous mice to generate *Gli3*<sup>X<sup>tl</sup>/+</sup>; *Cpk*<sup>+/-</sup> double heterozygous mice. Male or female *Gli3*<sup>X<sup>tl</sup>/+</sup>; *Cpk*<sup>+/-</sup> double heterozygous mice were then crossed with either *Cpk*<sup>+/-</sup> and the resulting litters were collected. All lines were maintained on a C57BL/6 background and housed in ventilated cages in a 12-h light/dark cycle and had ad libitum access to Teklad global 18% protein diet (2018, Inotiv, Huntington, UK) and water. Mice of both sexes were used for analysis with five mice in each experimental group as determined from power calculations to see a 30% difference in kidney/body weight (at 80% power, *p*=0.05) derived from our previous data using *Cpk* mice (Huang et al., 2016). Blood was collected via cardiac puncture and blood urea nitrogen (BUN) levels were quantified in plasma using the QuantiChrom™ Urea Assay Kit (BioAssay Systems, DIUR-100).

### 2.2 | Histological analysis

Histological analyses were performed on 5 μm periodic acid-Schiff stained sections. Slides were imaged using the Hamamatsu NanoZoomer slide scanner at 20× magnification. All analysis was conducted blinded on FIJI ImageJ software. The average area of individual cysts was determined using Image J particle analysis tool, with cysts defined as those >10,000 μm<sup>2</sup> in cross-sectional area (Huang et al., 2016). The cystic index (percentage of total cyst area/total kidney area), average cyst size, and number of cysts were then quantified.

### 2.3 | Generation of PKHD1-mutant human collecting duct cell lines by CRISPR/Cas9

Human collecting duct (HCD) cells were provided by Professor Pierre Ronco, Hopital Tenon, Paris, France, and originally derived from non-tumorous human kidney cortex, immortalized with SV-40 virus with clones selected that stained specifically for mAb272, a marker of collecting duct principal cells (Papadimitriou et al., 2020; Prie

et al., 1995; Valenti et al., 1996). HCD cells were maintained as previously described (Prie et al., 1995). Exon 5 of *PKHD1* was identified in the Leiden Open Variation Database (Fokkema et al., 2011) as a region to contain a high number of pathogenic variants in ARPKD patients. Therefore, a sgRNA was designed for exon 5 of *PKHD1* (5'-3' ACTTCCTGGAAGCATACTTC) and cloned into a pX330 plasmid (Addgene plasmid, 42230). HCD cells were transfected with the sgRNA encoding plasmid and pAcGFP1-C1 plasmid using FuGENE (Promega, E5911). After 48 h, fluorescence activated cell sorting (FACS) was performed to isolate GFP-positive cells and these were cultured for 2 weeks. Single cells were then seeded into 96-well plates by FACS, and clonal cell lines were expanded. Clones were genotyped by PCR of the targeted *PKHD1* genomic sequence and Sanger sequencing, using the following primers: 5'-3' ACTGCTGGGAATCCTTGTT and AGACACGCTGGCTCATTTACA. One *PKHD1*-mutant clonal cell line was generated, in addition to an isogenic wildtype control cell line that had undergone CRISPR transfection and cell sorting but no mutation in *PKHD1* was present.

### 2.4 | 3D spheroid assay

Matrigel (7.3 μL) (Corning, 356231) was mixed with 2.7 μL of 2000 cells in media on ice to a total volume of 10 μL which was added to the inner chamber of 15-well 3D μ-slides (ibidi, 81506) and left to set at 37°C for 30–40 min. Media (50 μL) was then added to each well and changed every 2 days. At Day 6, the cells were imaged on an Invitrogen EVOS M5000 Microscope at 20× magnification. Fifteen images were taken per well and 3 wells were imaged per condition or cell type. Experiments were repeated independently at least three times, 50 spheroids were quantified per experiment and a total number of 150–200 spheroids per condition were measured.

### 2.5 | Drug treatment

For inhibition of Hedgehog signaling, cells were treated with the SMO inhibitor cyclopamine (Chen et al., 2002). After cells were plated in Matrigel, the media added was supplemented with 10 μm cyclopamine (LKT Labs, C9710) and changed every 2 days.

### 2.6 | siRNA transfection

To lower *Gli3* levels in vitro, siRNA inhibition was used. The following conditions were used for each cell type:

non-transfected, non-targeting siRNA and *GLI3* siRNA. The following siRNAs were utilized: ON-TARGETplus non-targeting siRNA Control Pool (Dharmacon, D-001810-10-5) and ON-TARGETplus Human *GLI3* siRNA SMARTpool (Dharmacon, L-011043-00-0005). siRNA (30nM) was transfected into HCD cells using Lipofectamine RNAiMAX (Invitrogen, 56532) and cells were incubated at 37°C for 6 h. After 6 h, cells were prepared for the 3D spheroid assay or plated in 2D for RNA extraction after 6 days in culture.

## 2.7 | Quantitative RT-PCR

The RNeasy Plus Mini kit (Qiagen, 74134) and RNeasy Micro Kit (Qiagen, 74004) were used for mRNA extraction from murine tissue and HCD cells, respectively. cDNA was prepared using the iScript gDNA Clear cDNA Synthesis kit (BioRad, 172-5034) as per the manufacturer's instructions. Quantitative real-time polymerase chain reaction (qRT-PCR) was performed in duplicate using the qPCRBIO SyGreen Mix Lo-ROX (PCRBioSystems, PB20.11) with gene specific primers (*Ihh*, *Shh*, *Ptch1*, *Smo*, *Sufu*, *Gli1*, *Gli2*, and *Gli3/GLI3*) normalized to the housekeeping gene (*Gapdh/GAPDH*).

## 2.8 | Western blotting

Protein lysates were prepared from 14-day postnatal kidneys by homogenization in radioimmunoprecipitation assay (RIPA) buffer (Merck, 20-188) with 40 µL/mL cOmplete™ EDTA-free Protease Inhibitor Cocktail (Sigma, 1167498001) and 10 µL/mL sodium orthovanadate phosphatase inhibitor (Merck, S6508-50G). Protein lysates (50 µg) were run on a 7.5% Mini-PROTEAN TGX Precast gel (Bio-Rad) and transferred to polyvinylidene fluoride (PDVF) membranes (Millipore, IPVH00010). Membranes were blocked in 5% milk, 0.1% bovine serum albumin (BSA) in 0.1% Tween-20 in PBS, and incubated in the following antibodies overnight at 4°C: Goat anti-GLI3 (1 µg/mL, R&D Systems, no. AF3690) or Rabbit anti-alpha-tubulin (1 µg/mL, Abcam, ab4074). Membranes were then incubated in the appropriate anti-goat (DAKO, P044901) or anti-rabbit (DAKO, P044801) horseradish peroxidase (HRP)-conjugated secondary antibodies (1:2000) for 1 h at room temperature and proteins were visualized by chemiluminescent imaging, using ECL Western Blotting Substrate (Amersham, RDN2232). Densitometry of the 190 kDa full-length GLI3 (GLI3A) and 83 kDa truncated GLI3 (GLI3R) protein bands were calculated relative to α-tubulin on FIJI ImageJ software. Total GLI3 was

calculated as total GLI3A and GLI3R protein and the ratio of GLI3A:GLI3R was quantified.

## 2.9 | Statistical analysis

All statistical analyses were performed using GraphPad PRISM. All data were plotted as mean value ± standard deviation (SD). Normality was assessed by Shapiro–Wilk test and normally distributed data were analyzed by an unpaired *t*-test for comparisons between two groups and a one-way ANOVA with Tukey's multiple comparisons test for comparisons with more than two groups. For data not normally distributed, data were analyzed using a Mann–Whitney *U*-test for comparisons between two groups and Kruskal–Wallis test with Dunn's multiple comparison test for comparisons with more than two groups. For in vitro experiments with two variables, such as cell type and treatment group, a two-way ANOVA with Tukey's multiple comparison test was utilized.

## 3 | RESULTS

### 3.1 | *Gli3* levels are elevated in the cystic kidneys of the *Cpk* model

Firstly, we examined the levels of components of the Hh signaling pathway in the *Cpk* mouse model, which replicates the pathophysiology of ARPKD (Avner et al., 1987, 1988; Hou et al., 2002). In this model, cystogenesis initiates during embryogenic development with the presence of tubular dilations which rapidly progress to renal cysts in the collecting ducts from birth through to postnatal day 21, resembling the phenotype of rapid cyst development seen in the human disease (Avner et al., 1987). We measured the transcript levels of Hh pathway genes in whole kidneys from *Cpk*<sup>-/-</sup> mice and their wildtype littermates at postnatal (P) 10, P14, and P21, when cysts are present within the tissue (Figure 1a). No significant differences were detected at any timepoint in the levels of either of the Hh ligands known to be expressed in the kidney *Ihh* and *Shh* (Greenberg et al., 2023) or the downstream Hh pathway genes, *Ptch1*, *Smo*, *Sufu*, *Gli1*, or *Gli2* between *Cpk*<sup>+/+</sup> and *Cpk*<sup>-/-</sup> mice (Figure 1b–d). Notably, the transcription factor *Gli3* was significantly upregulated in *Cpk*<sup>-/-</sup> mice at both P14 by 2.7-fold and P21 by 3.5-fold in comparison with *Cpk*<sup>+/+</sup> mice (Figure 1c,d, P14 *p* = 0.005, P21 *p* = 0.002). Prior to this, at P10 there is a slight increase in *Gli3* transcript levels with a 1.3-fold change, although this is not significantly different at this timepoint (Figure 1b, *p* = 0.330). The upregulation of *Gli3* transcript between

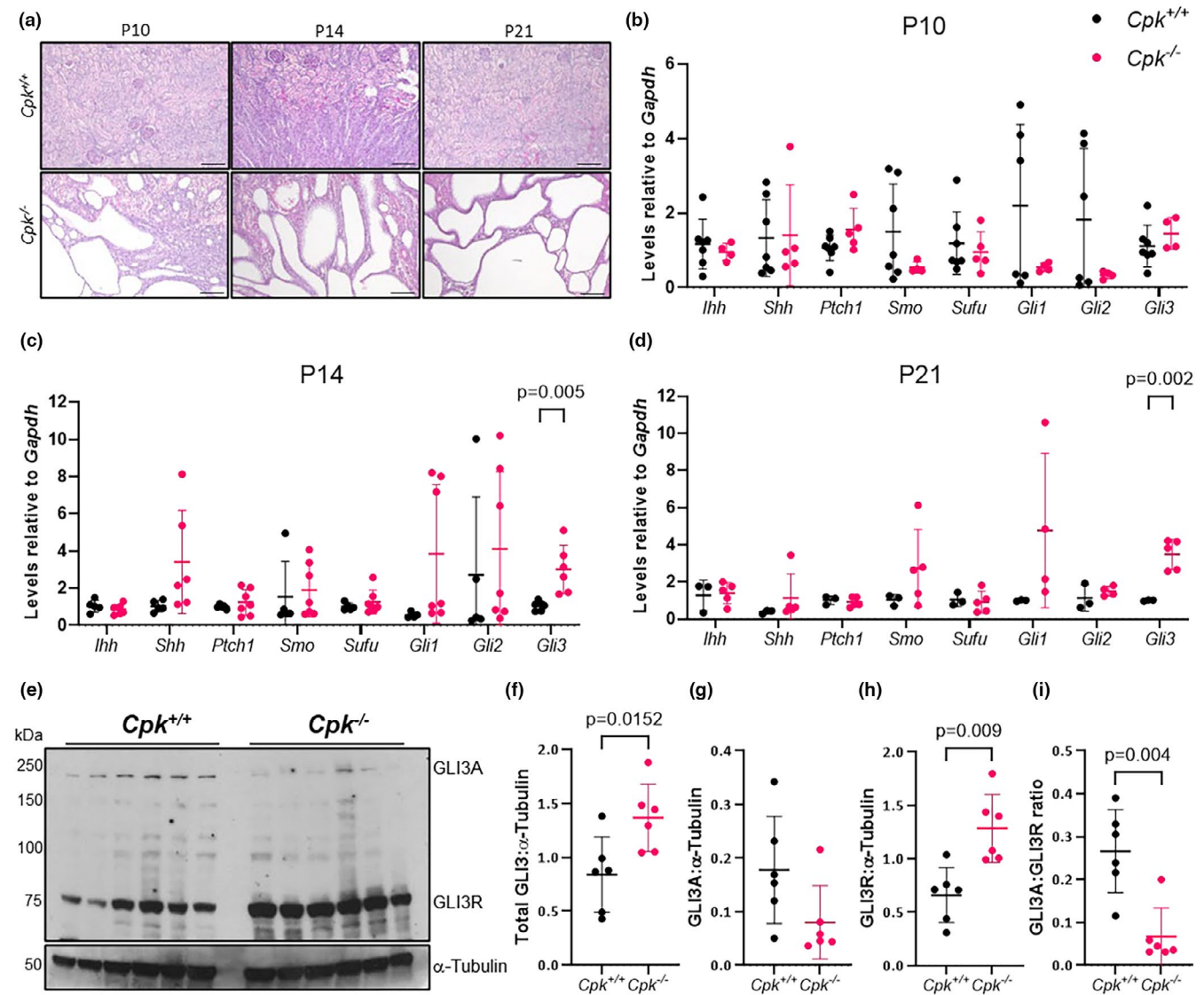


**FIGURE 1** *Gli3* is elevated at both the transcript and protein level in the cystic kidneys of  $Cpk^{-/-}$  mice. (a) Representative images of periodic acid-Schiff staining on 5  $\mu\text{m}$  sections of  $Cpk^{+/+}$  and  $Cpk^{-/-}$  kidneys at P10, P14, and P21. Images taken at 10x magnification. Scale bars: 100  $\mu\text{m}$ . Quantitative RT-PCR analysis of *Ihh*, *Shh*, *Ptch1*, *Smo*, *Sufu*, *Gli1*, *Gli2*, and *Gli3* transcript levels relative to *Gapdh* from whole kidney RNA from  $Cpk^{+/+}$  and  $Cpk^{-/-}$  mice at (b) P10, (c) P14, and (d) P21. Ct values of each gene of interest were normalized to littermate controls at each timepoint (Unpaired *t*-test,  $n=7, 5, 3$  for  $Cpk^{+/+}$ ,  $n=4, 6, 5$  for  $Cpk^{-/-}$  mice at P10, P14, and P21, respectively). (e) Western blot analysis of the levels of full-length GLI3 activator (GLI3A) and truncated GLI3 repressor (GLI3R) in P14 kidney lysates from  $Cpk^{+/+}$  ( $n=6$ ) and  $Cpk^{-/-}$  ( $n=6$ ). (f) The relative intensity of total GLI3, a sum of GLI3A and GLI3R, (g) GLI3A and (h) GLI3R were quantified by densitometry in arbitrary units relative to endogenous alpha-tubulin. (i) The ratio of GLI3A:GLI3R was quantified (Mann-Whitney *t*-test,  $n=6$  mice per group). Data represents mean  $\pm$  SD.

P10 and P14 is in line with the period of rapid cyst progression observed in this model.

The balance between full-length activator GLI3A and repressor GLI3R protein is critical in determining the cellular function of Hh signaling (Matissek & Elswa, 2020). Therefore, the protein levels of GLI3A and GLI3R were analyzed by Western blotting in 14-day old  $Cpk^{-/-}$  and wildtype littermates. Total GLI3 protein levels, a sum of both GLI3A and GLI3R protein, and GLI3R protein levels were significantly increased

in  $Cpk^{-/-}$  mice (Figure 1e,f,  $p=0.0152$  and  $p=0.009$ , respectively). Although, there is a trend toward reduced GLI3 activator protein levels in  $Cpk^{-/-}$  mice compared with wildtype controls, this was not significant (Figure 1h,  $p=0.065$ ). There was a significant decrease in the ratio of GLI3 activator to GLI3 repressor in  $Cpk^{-/-}$  mice, further demonstrating an increase in the relative levels of GLI3 repressor (Figure 1i,  $p=0.004$ ). Collectively, these data suggest there is enhanced transcript levels of *Gli3*, alongside an increase in the total

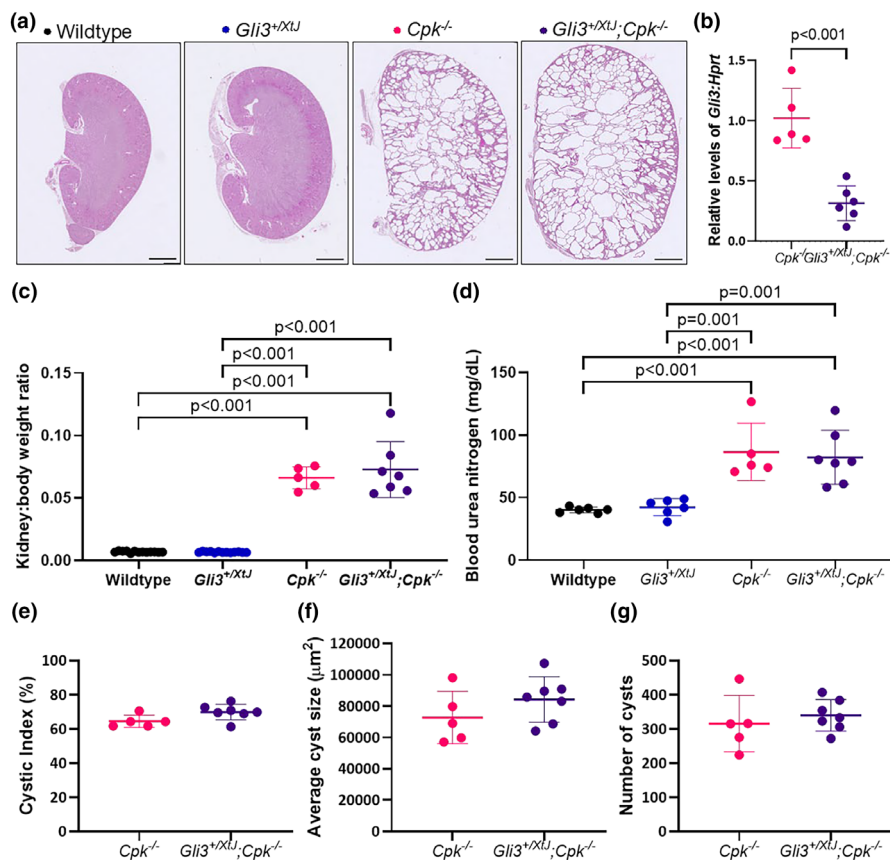


**FIGURE 2** Reduced levels of *Gli3* have no effect on cyst progression in *Cpk* mice. (a) Representative images of periodic acid-Schiff (PAS) staining on 5  $\mu\text{m}$  sections of wildtype, *Gli3<sup>+XtJ</sup>*, *Cpk<sup>-/-</sup>*, and *Gli3<sup>+XtJ</sup>; Cpk<sup>-/-</sup>* kidneys at P14. 10 $\times$  magnification, scale bars: 1 mm. (b) Quantitative RT-PCR analysis of *Gli3* relative to *Hprt* from whole kidney RNA at P14. Relative Ct values of each gene of interest were normalized to *Cpk<sup>-/-</sup>* littermates (Unpaired *t*-test). (c) Kidney: Body weight ratio and (d) blood urea nitrogen (BUN) levels for each group. One-way ANOVA with Tukey's multiple comparisons test. Quantification of PAS staining was performed on *Cpk<sup>-/-</sup>* and *Gli3<sup>+XtJ</sup>; Cpk<sup>-/-</sup>* mice to determine (e) cystic index, the percentage of total cyst area/total kidney area, (f) average cyst size ( $\mu\text{m}^2$ ) and (g) total number of cysts per kidney section. Cysts were defined as  $\geq 10,000 \mu\text{m}^2$ . Unpaired *t*-test. Data represents mean  $\pm$  SD.  $n = 6$  for wildtype,  $n = 6$  for *Gli3<sup>+XtJ</sup>*,  $n = 5$  for *Cpk<sup>-/-</sup>*, and  $n = 7$  for *Gli3<sup>+XtJ</sup>; Cpk<sup>-/-</sup>* mice.

level of GLI3 protein. Additionally, a shift toward the processing of GLI3 full length activator protein to the truncated repressive form is observed in cystic kidneys in the *Cpk* model of ARPKD.

### 3.2 | Reduction of *Gli3* does not alter the cystic phenotype in *Cpk<sup>-/-</sup>* mice

We subsequently hypothesized that elevated Gli3 may be driving cystogenesis in ARPKD and that preventing this increase could reduce disease severity. To test this, we modulated *Gli3* levels genetically in the *Cpk* model using mice harboring a *Gli3<sup>XtJ</sup>* allele, which contains a loss-of-function *Gli3* mutation (Hui & Joyner, 1993). As the *Gli3<sup>XtJ/XtJ</sup>* mouse is embryonic lethal (Hui & Joyner, 1993), we reduced *Gli3* levels in the *Cpk* mouse using a heterozygous *Gli3<sup>+XtJ</sup>* haploinsufficiency model. We crossed

*Gli3<sup>+XtJ</sup>; Cpk<sup>+/-</sup>* double heterozygous mice with *Cpk<sup>+/-</sup>* mice and collected *Gli3<sup>+XtJ</sup>; Cpk<sup>-/-</sup>* offspring and littermates at P14 (Figure 2a). The loss of one *Gli3* allele was sufficient to significantly reduce *Gli3* transcript levels in *Gli3<sup>+XtJ</sup>; Cpk<sup>-/-</sup>* mice by 69% relative to *Cpk<sup>-/-</sup>* littermates (Figure 2b,  $p < 0.001$ ). However, no changes were observed in the kidney: body weight ratio or BUN levels between *Cpk<sup>-/-</sup>* and *Gli3<sup>+XtJ</sup>; Cpk<sup>-/-</sup>* mice (Figure 2c,d). Analysis of the cystic phenotype of these mice showed no differences in cystic index between *Cpk<sup>-/-</sup>* and *Gli3<sup>+XtJ</sup>; Cpk<sup>-/-</sup>* kidneys, with a mean value of  $64.5 \pm 3.6\%$  and  $69.9 \pm 4.5\%$  respectively (Figure 2a,e). Additionally, no difference was observed in the average cyst size or number of cysts between *Gli3<sup>+XtJ</sup>; Cpk<sup>-/-</sup>* mice and *Cpk<sup>-/-</sup>* mice (Figure 2f,g). These data suggest that although *Gli3* is elevated in the cystic kidneys of *Cpk* mice, decreasing the level of *Gli3* does not alter the ARPKD cystic phenotype of the *Cpk* mouse.

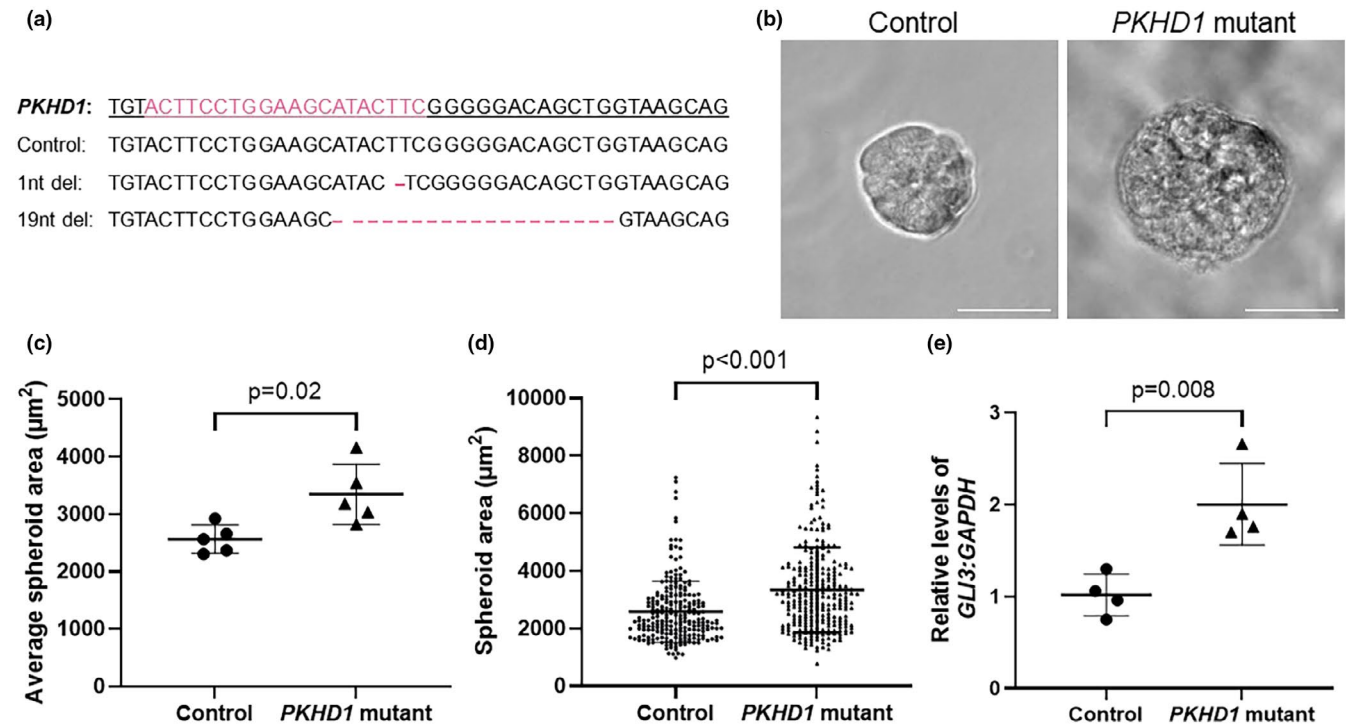


**FIGURE 3** Generation of a human in vitro model of *PKHD1*-mutant spheroids. (a) CRISPR-Cas9 was utilized to generate mutations within exon 5 of *PKHD1* in a human collecting duct cell line. Alignment of Sanger sequencing data of *PKHD1* exon 5 from clonal cell lines generated was analyzed using Synthego ICE analysis. *PKHD1* wildtype sequence is underlined and sgRNA-binding site is highlighted in pink. Nucleotide deletion sites are indicated with a dash. (b) Representative images of isogenic wildtype control and *PKHD1*-mutant 3D spheroids formed in Matrigel following 6 days in culture. (c) The cross-sectional area of each spheroid was quantified, and the average spheroid area was calculated for each independent repeat. (d) Area of each individual spheroid quantified across all repeats.  $n = 5$  independent repeats. (e) Quantitative RT-PCR analysis of *GLI3* relative to *GAPDH* from RNA extracted from isogenic wildtype control and *PKHD1*-mutant HCD cells cultured for 6 days. Relative Ct values of each gene of interest were normalized to isogenic wildtype control HCD cells. Data represent mean  $\pm$  SD. Unpaired *t*-test.  $n = 4$  independent repeats.

### 3.3 | Generation of a 3-dimensional *PKHD1*-mutant human spheroid model

To further investigate the possible role of *GLI3* in the pathogenesis of ARPKD, we generated a *PKHD1*-mutant HCD cell line using CRISPR-Cas9. We utilized CRISPR-Cas9 to target exon 5 of *PKHD1*, a region identified to have a high number of pathogenic variants reported in ARPKD patients in the Leiden Open Variation Database (Fokkema et al., 2011). We generated an isogenic clone with no mutations in the *PKHD1* gene following transfection and a clone with a compound heterozygous mutation in *PKHD1*, with a single nucleotide deletion in one allele and 19 nucleotide deletion in the other allele (Figure 3a). Both frameshift deletions are predicted to result in a premature stop codon and result in a truncated *PKHD1* protein. We analyzed the effect of this *PKHD1* mutation on in vitro spheroid size. Cells from both lines were embedded in Matrigel and cultured for 6 days until 3D spheroids had formed. We observed significantly larger spheroids in the *PKHD1*-mutant HCD line, with a greater average spheroid area ( $3349 \pm 524 \mu\text{m}^2$ ) when compared

with the isogenic control HCD cell line ( $2564 \pm 246 \mu\text{m}^2$ ) (Figure 3b,c,  $p = 0.02$ ). Additionally, the *PKHD1*-mutant HCD cell line form significantly larger individual spheroids than isogenic control cells, with the largest *PKHD1*-mutant spheroids measured at  $>8000 \mu\text{m}^2$  compared with a maximum spheroid size of  $7250 \mu\text{m}^2$  for isogenic control spheroids (Figure 3d,  $p < 0.001$ ). We found significantly elevated *GLI3* transcript levels in *PKHD1*-mutant HCD cells, increased by twofold, as compared with isogenic control HCD cells (Figure 3e,  $p = 0.008$ ). This mirrors the findings observed in the *Cpk* mouse model of ARPKD, where increased levels of *Gli3* transcript levels were detected in cystic mice.

### 3.4 | Reduction of *GLI3* does not reduce the size of *PKHD1*-mutant spheroids

We next aimed to analyze the effect of Hh pathway inhibition on spheroid size in *PKHD1*-mutant HCDs. Initially, we inhibited Hh pathway activity using the SMO inhibitor,

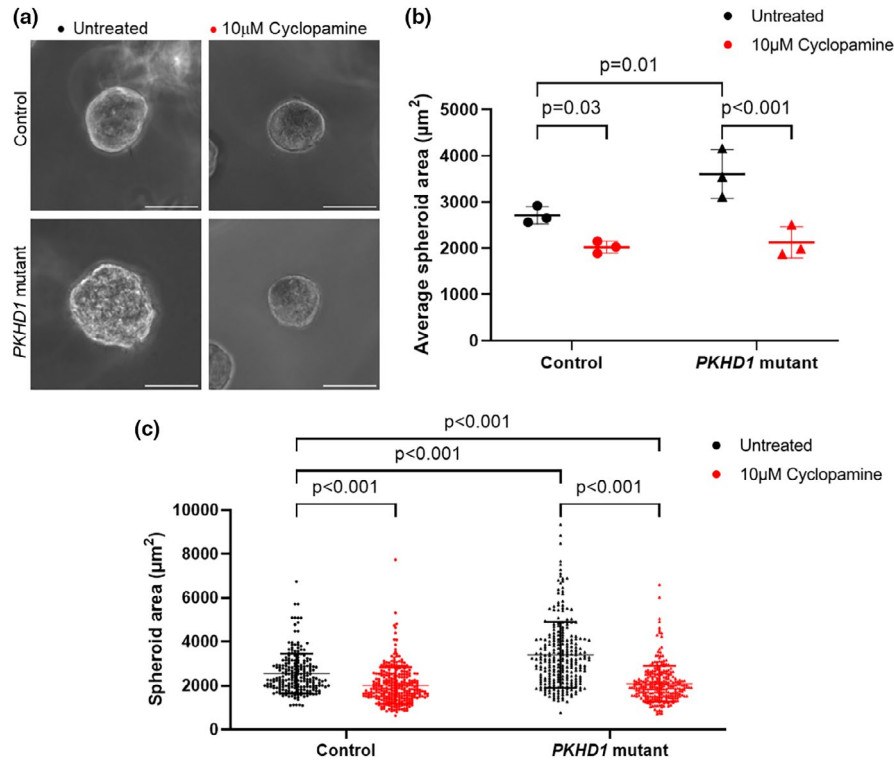


**FIGURE 4** Cyclopamine treatment inhibits *PKHD1*-mutant spheroid size in vitro. Isogenic wildtype control and *PKHD1*-mutant HCD cells were embedded in Matrigel and cultured for 6 days to generate 3D spheroids. Cells were left untreated or treated with 10 μM cyclopamine, a SMO inhibitor, every 2 days. (a) Representative images of isogenic wildtype control and *PKHD1*-mutant spheroids at day 6, following 10 μM cyclopamine treatment. (b) The cross-sectional area of each spheroid was quantified, and the average spheroid area was calculated for each independent repeat. (c) Area of each individual spheroid quantified across all repeats.  $n = 3$  independent repeats. Data represent mean  $\pm$  SD. Two-way ANOVA with Tukey's multiple comparisons test. Statistical comparisons are shown relative to the untreated isogenic wildtype control and between conditions of the same cell type.

cyclopamine, in both isogenic control and *PKHD1*-mutant HCD cells (Figure 4a). Treatment with 10 μM cyclopamine for 6 days significantly reduced average spheroid size in both isogenic control and *PKHD1*-mutant cells in comparison to untreated cells (Figure 4b,c,  $p = 0.03$  and  $p < 0.001$ ). We subsequently examined the effect of modulating *GLI3* transcript levels on spheroid size in both isogenic control and *PKHD1*-mutant HCD cells. To reduce the levels of *GLI3* transcript, HCD cell lines were transfected with *GLI3* siRNA prior to plating in Matrigel. Cells were either left untransfected or transfected with 30 nM of either non-targeting siRNA or *GLI3* siRNA. Transfection with the *GLI3* siRNA significantly reduced *GLI3* transcript levels by 0.55-fold in *PKHD1*-mutant HCD cells, down to similar levels observed in control HCD cells (Figure 5a,  $p = 0.02$ ). In isogenic control cells, *GLI3* transcript levels were reduced by an average of 0.61-fold, however the level of knockdown was variable and not significantly different (Figure 5a). Although *GLI3* siRNA reduced *GLI3* transcript levels in *PKHD1*-mutant cells, it did not influence spheroid size with no significant difference in average spheroid area between all experimental conditions for the *PKHD1*-mutant cell line (Figure 5b,c). There was also no

significant difference in spheroid area between any of the conditions for the isogenic control cell line (Figure 5b,c).

Thus, we have demonstrated that *Gli3* is significantly upregulated in the *Cpk* mouse and a human *PKHD1*-mutant clonal collecting duct cell line. Additionally, we have demonstrated that reducing the transcript levels of *Gli3/GLI3* levels in both of these contexts does not alter disease progression or spheroid size respectively, suggesting it is not required for ARPKD.

## 4 | DISCUSSION

Despite studies observing an increase in Hh pathway levels in both in vitro and in vivo models of ADPKD, as well as in human ADPKD tissue, (Chan et al., 2010; Jonassen et al., 2012; Tran et al., 2014) there has been a lack of research regarding the role of Hh in murine and human ARPKD. Our findings have bridged this gap by identifying a significant upregulation of the Hh transcriptional effector *Gli3* in the *Cpk* mouse. Elevation of *Gli3* transcript was in line with the period of rapid cyst progression at the later stages of the disease at P14 to P21. This provides



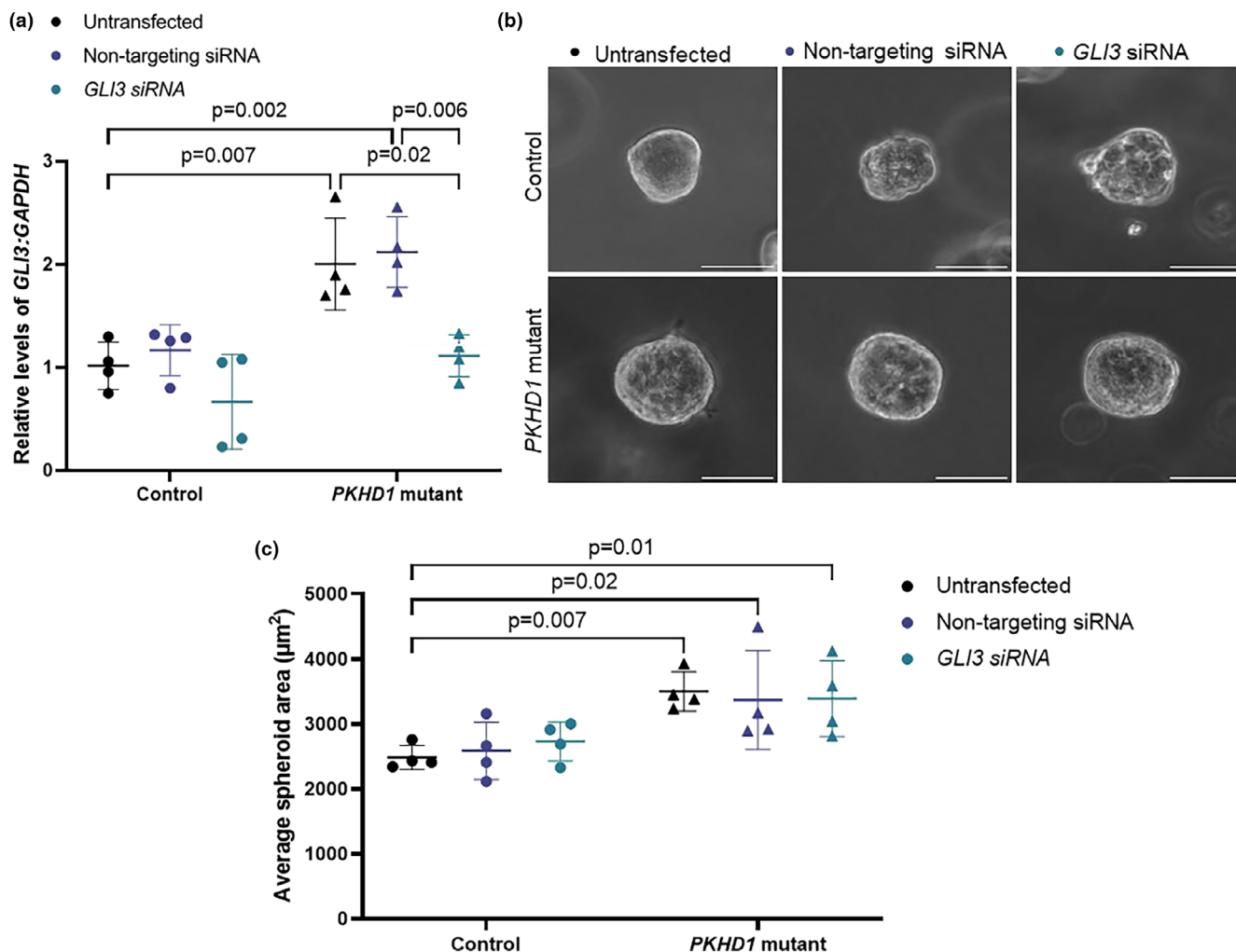


**FIGURE 5** *GLI3* knockdown does not alter size of *PKHD1*-mutant spheroids. Isogenic wildtype control and *PKHD1*-mutant cells were transfected with non-targeting siRNA or *GLI3* siRNA and embedded in Matrigel to generate spheroid structures. (a) Quantitative RT-PCR analysis of *GLI3* relative to *GAPDH* from RNA extracted from control and *PKHD1*-mutant HCD cells for all conditions 6 days after transfection. Relative Ct values of each gene of interest were normalized to untreated isogenic control HCD cells. (b) Representative images of isogenic control and *PKHD1*-mutant 3D spheroids that were not transfected or transfected with non-targeting siRNA or *GLI3* siRNA. Images of the spheroids were taken at Day 6 at 20 $\times$  magnification. (c) The cross-sectional area of each spheroid was quantified, and the average spheroid area was calculated for each independent repeat. Data represent mean  $\pm$  SD. Two-way ANOVA with Tukey's multiple comparisons test. Statistical comparisons are shown relative to the untransfected isogenic wildtype control and between conditions of the same cell type.

the first evidence of *Gli3* upregulation in an ARPKD murine model, paralleling data in ADPKD models and renal cystic mouse models caused by mutations in ciliary genes (Jonassen et al., 2012; Li et al., 2016; Tran et al., 2014). Similar to our findings, upregulation of the Hh pathway in other cystic mouse models, including *Gli3*, has only been observed at the more advanced stages of the disease (Jonassen et al., 2012; Li et al., 2016). In this study we also detected *GLI3* upregulation in a newly developed human *PKHD1*-mutant cellular model, mimicking the findings in *Cpk* mice.

Further to this, we found an increase in the total *GLI3* protein level in *Cpk* mice at P14. Within the cell, *GLI3* can

act as either a transcriptional activator (*GLI3A*) or transcriptional repressor (*GLI3R*) dependent on the activity of the Hh pathway in a context dependent manner (Matissek & Elswa, 2020). In the *Cpk* model, we detected increased processing of *GLI3A* to *GLI3R*, with a tendency for reduced levels of *GLI3A* and elevated levels of *GLI3R*, indicating Hh pathway inhibition in the highly cystic kidneys of *Cpk* mice. The importance of elevated *GLI3R* was not explored in this study, but previous work has shown that this can lead to severe pathological effects in the kidney during its development. In mice, the global overexpression of *GLI3R* causes severe renal developmental abnormalities, with mice displaying hydronephrosis, hydroureter, and hydronephrosis

and some mutants having a bi-lobed kidney with a single ureter (Blake et al., 2016). Pallister-Hall syndrome (PHS) is associated with truncating mutations in *GLI3*, which leads to the production of a constitutively active GLI3R-like protein (Johnston et al., 2005; McClelland et al., 2022). Around 27% of PHS patients have renal developmental abnormalities, most frequently these patients present with phenotypes such as hypoplasia or agenesis (McClelland et al., 2022).

A common feature of PKD pathogenesis is an increase in cAMP levels, leading to the activation of kinases such as PKA or GSK3 $\beta$ , key regulators of GLI3 processing to GLI3R (Bergmann et al., 2018; Briscoe & Therond, 2013). It could be hypothesized that enhanced activity of kinases such as PKA or GSK3 $\beta$ , which is a common feature of PKD pathogenesis (Kakade et al., 2016; Tao et al., 2015; Ye et al., 2017), may increase GLI3 processing in the context of PKD. Previous studies have shown that overactivation of PKA activity within the context of PKD, leads to elevation of GLI3R and reduced GLI1 protein (Ye et al., 2017). These authors suggested that the enhanced GLI3R activity may contribute to the cystic phenotype, with mice exhibiting elevated GLI3R caused by constitutive PKA activation developing more severe PKD (Ye et al., 2017).

Following on from the identification of increased levels of *Gli3*, the effect of modulating the levels of *Gli3* was assessed in the *Cpk* mouse model of ARPKD and in *PKHD1*-mutant spheroids. Utilizing a *Gli3* haploinsufficiency model, *Gli3* transcript levels were significantly reduced in *Cpk* mice, although this did not alter the cystic phenotype of *Cpk* mice. To further interrogate the function of *GLI3* in the pathogenesis of ARPKD, a *PKHD1*-mutant spheroid model was then utilized. Initially, the Hh pathway was inhibited using the SMO-inhibitor cyclopamine, which reduced spheroid size in control and *PKHD1*-mutant HCDs. Pharmacological inhibition of SMO reduces cystogenesis in other in vitro PKD models, including metanephric cystic explants and human primary ADPKD cells, as well as in vivo in the *Pck* rat model of ARPKD (Chan et al., 2010; Sato et al., 2018; Silva et al., 2018; Tran et al., 2014). However, a specific reduction of *GLI3* transcript levels using siRNA did not alter spheroid size in *PKHD1*-mutant HCD cells.

The variation in in vitro spheroid size observed after treatment with cyclopamine, compared with *GLI3* siRNA inhibition, can likely be attributed to cyclopamine's more comprehensive inhibition of the Hh pathway. By antagonizing SMO, cyclopamine reduces the level of GLI1 and GLI2 (Hu et al., 2006), which may be key to modulating spheroid size in this model. Additionally, cyclopamine can have off target functions and has previously been

demonstrated to inhibit growth and induce apoptosis, independently of SMO/GLI inhibition (Meyers-Needham et al., 2012; Zhang et al., 2009). Thus, the changes observed in spheroid size following cyclopamine treatment are likely due to the broader effect on the Hh pathway or off-target effects.

Although, pharmacological modulation of the Hh pathway has been demonstrated to reduce cystogenesis both in vitro in this study and in vitro and in vivo in previous reports (Chan et al., 2010; Hsieh et al., 2022; Sato et al., 2018; Tran et al., 2014), there is limited data suggesting that the genetic modulation of this pathway alters PKD cystogenesis (Ma et al., 2019; Tran et al., 2014). Prior studies have not investigated the modulation of *GLI3* specifically in cellular models of either ADPKD or ARPKD. Genetic manipulation of *Gli3* in epithelial cells has previously been analyzed in the context of murine ADPKD. The loss of *Gli2* and *Gli3* did not alter cyst formation caused by mutations in *Pkd1*, indicating that the downstream Hh transcription factors, *Gli2* and *Gli3*, have no role within the tubular epithelium in mediating cystogenesis in ADPKD (Ma et al., 2019). This matches the findings in this report which demonstrated no difference in disease progression in *Cpk* mice or spheroid size in *PKHD1*-mutant cells following *Gli3* global repression.

A key limitation of this study is the level of *GLI3* downregulation achieved with these models. It should be considered that complete abrogation of the gene might impact cyst formation and progression, however this was not feasible in our in vivo model. *Gli3*<sup>XI/XI</sup> mice are embryonic lethal and therefore it is not possible to analyze mice with a complete loss of *Gli3* expression postnatally (Johnson, 1967). In our in vitro model, siRNA inhibition was able to reduce the levels of *GLI3* down to that observed in controls, although techniques like CRISPR-Cas9 may be of use to study the total loss of *GLI3* in this context. Additionally, as *GLI3R* protein levels were elevated in *Cpk* mice, another approach could be to study the effect of altering the level of *GLI3R* on cyst formation and progression in the context of ARPKD. It would also be informative to assess how *Gli3* downregulation alters other Hh components to fully understand the effects on the whole signaling pathway.

A significant obstacle to advancing our understanding of the pathogenic mechanisms involved in ARPKD is the absence of genetically relevant models of ARPKD (Hiratsuka et al., 2022). The renal phenotype of *Pkhd1*-mutant mice differs from the presentation of ARPKD in humans, varying from a complete absence of kidney disease to slowly progressing late-onset renal cysts (Ishimoto et al., 2023; Williams et al., 2008; Woollard

et al., 2007; Yang et al., 2023), thus *Cpk* mice are widely used to model ARPKD (Chiu et al., 2006; Huang et al., 2016). Although the *Cpk* mouse does not contain mutations in *Pkhd1* as seen in patients, the levels of fibrocystin protein are reduced by 90% in *Cpk* kidneys, as well as in cystin-depleted renal cortical collecting duct cells (Zhang et al., 2023). The levels of fibrocystin can be partially restored in *Cpk* mice with the collecting duct-specific expression of a cystin-GFP fusion protein, indicating a role for cystin in maintaining fibrocystin levels (Zhang et al., 2023).

Lastly, this report describes the development of a human cellular model of ARPKD. In recent years, there has been progress in the development of cellular ARPKD models as a complementary approach to mouse models. *PKHD1*<sup>-/-</sup> ureteric epithelial cells isolated from human iPSC kidney organoids spontaneously form cyst-like structures when induced to form ureteric bud stalks (Howden et al., 2021). Additionally, two studies have described the use of organoids derived from ARPKD patient-derived iPSCs, although these did not reliably form cysts without cAMP stimulation. Moreover, in both studies these cystic tubules formed in LTL+ proximal tubules with only some developing in CDH1+ distal nephron regions (Hiratsuka et al., 2022; Low et al., 2019). CRISPR-Cas9 has also been employed in iPSCs to produce a *PKHD1*-mutant ARPKD kidney organoid-on-a-chip model. Organoids were exposed to fluid-flow on 3D millifluidic chips, resulting in the formation of cyst-like structures in distal nephrons only in *PKHD1*<sup>-/-</sup> organoids and not in *PKHD1*<sup>+/-</sup> organoids (Hiratsuka et al., 2022).

We have described a novel human *PKHD1*-mutant cellular spheroid model, which can complement current ARPKD organoid models. This *PKHD1*-mutant cell line contains a compound heterozygous *PKHD1* mutation in a region of the gene which contains several pathogenic variants in patients (Fokkema et al., 2011). Compound heterozygous mutations occur in the majority of ARPKD cases (Bergmann et al., 2005; Burgmaier et al., 2021), thus this *PKHD1*-mutant line is a valuable model. The *PKHD1*-mutant collecting duct cells form larger spheroids in 3D culture than isogenic controls over 6 days without the need of additional stimulation or fluid flow. In future studies, it may be beneficial to enhance this phenotype, such as through forskolin addition, to stimulate cAMP (Sharma et al., 2019). A key advantage of this model is the formation of collecting duct spheroid structures, which is the primary cell type in which cysts form in patients with ARPKD (Bergmann et al., 2018). However, a limitation of the assay is that it lacks the

cellular complexity and microenvironment that would be present in ARPKD tissue, such as the vasculature, immune or surrounding interstitial cells, which are important to fully mimic the cystic environment. Additionally, these *PKHD1*-mutant spheroids are responsive to drug treatment as demonstrated using the drug cyclopamine. Hence, this cellular model is highly valuable due to its ease of use and scalability as well as having the potential to be utilized in applications such as high-throughput drug screening, facilitating the evaluation of novel therapeutic interventions.

Overall, we have demonstrated that although levels of GLI3 are enhanced in models of ARPKD, dampening this upregulation does not alter cyst progression or spheroid size in mouse and human models respectively, highlighting the functional complexity of the Hh pathway in ARPKD. In addition, we have developed a *PKHD1*-mutant spheroid model which provides a crucial resource for studying the pathogenesis of the disease, as well as discovering novel therapeutic targets and drugs aimed at addressing the needs of individuals with ARPKD.

#### AUTHOR CONTRIBUTIONS

L.G.R., N.D.R., P.J.W., and D.A.L. conceived and designed the study. L.G.R. and M.K.J. acquired mouse material. T.C. provided the *Gli3*<sup>X<sup>fl</sup></sup> mouse line. L.G.R. performed mouse husbandry, qRT-PCR, Western blotting, renal function assays and histology, with assistance from M.K.J., L.W., J.C.C., and C.J.R. N.P.T., G.S., and K.L.P. designed the guide RNAs and generated the CRISPR plasmids. L.G.R. generated and characterized the *PKHD1*-mutant cell line and performed drug and siRNA treatments. L.G.R. collated the data and presented the figures. L.G.R. and D.A.L. wrote the manuscript, and subsequently all authors were involved in revision and preparation of the final manuscript.

#### ACKNOWLEDGMENTS

L.G.R. was supported by a Kidney Research UK (KRUK) PhD studentship (ST\_006\_20181123) and a University College London Research Culture Award. This work was also supported by a Wellcome Trust Investigator Award (220895/Z/20/Z) and a BBSRC International Partnership Institutional Award (BB/X512011/1) to D.A.L., as well as a Canadian Institutes of Health Research Foundation Grant to N.D.R. The authors would like to thank Professor Pierre Ronco (Hopital Tenon, Paris, France) for providing the human collecting duct cell line.

#### CONFLICT OF INTEREST STATEMENT

The authors declare no conflicts of interest.

## DATA AVAILABILITY STATEMENT

The data that support the findings of this study are available from the corresponding author upon reasonable request.

## ETHICS STATEMENT

All experiments were carried out in accordance with the UK Animals (Scientific Procedures) Act 1986 and the ARRIVE guidelines with both Home Office and institutional ethical approval (University College London Local Ethics Committee).

## ORCID

David A. Long  <https://orcid.org/0000-0001-6580-3435>

## REFERENCES

- Avner, E. D., Studnicki, F. E., Young, M. C., Sweeney, W. E., Jr., Piesco, N. P., Ellis, D., & Fettermann, G. H. (1987). Congenital murine polycystic kidney disease. *Pediatric Nephrology*, *1*, 587–596.
- Avner, E. D., Sweeney, W. E., Young, M. C., & Ellis, D. (1988). Congenital murine polycystic kidney disease. II. Pathogenesis of tubular cyst formation. *Pediatric Nephrology*, *2*, 210–218.
- Bangs, F., & Anderson, K. V. (2017). Primary cilia and mammalian hedgehog signaling. *Cold Spring Harbor Perspectives in Biology*, *9*, a028175.
- Bergmann, C., Guay-Woodford, L. M., Harris, P. C., Horie, S., Peters, D. J. M., & Torres, V. E. (2018). Polycystic kidney disease. *Nature Reviews Disease Primers*, *4*(1), 50.
- Bergmann, C., Senderek, J., Windelen, E., Küpper, F., Middeldorf, I., Schneider, F., Dornia, C., Rudnik-Schöneborn, S., Konrad, M., Schmitt, C. P., Seeman, T., Neuhaus, T. J., Vester, U., Kirfel, J., Büttner, R., & Zerres, K. (2005). Clinical consequences of PKHD1 mutations in 164 patients with autosomal-recessive polycystic kidney disease (ARPKD). *Kidney International*, *67*, 829–848.
- Blake, J., Hu, D., Cain, J. E., & Rosenblum, N. D. (2016). Urogenital development in Pallister-hall syndrome is disrupted in a cell-lineage-specific manner by constitutive expression of GLI3 repressor. *Human Molecular Genetics*, *25*, 437–447.
- Briscoe, J., & Thérond, P. P. (2013). The mechanisms of hedgehog signalling and its roles in development and disease. *Nature Reviews. Molecular Cell Biology*, *14*, 416–429.
- Burgmaier, K., Brinker, L., Erger, F., Beck, B. B., Benz, M. R., Bergmann, C., Boyer, O., Collard, L., Dafinger, C., Fila, M., Kowalewska, C., Lange-Sperandio, B., Massella, L., Mastrangelo, A., Mekahli, D., Miklaszewska, M., Ortiz-Bruechle, N., Patzer, L., Prikhodina, L., ... Nalcacioglu, H. (2021). Refining genotype–phenotype correlations in 304 patients with autosomal recessive polycystic kidney disease and PKHD1 gene variants. *Kidney International*, *100*, 650–659.
- Chan, S.-K., Riley, P. R., Price, K. L., McElduff, F., Winyard, P. J., Welham, S. J. M., Woolf, A. S., & Long, D. A. (2010). Corticosteroid-induced kidney dysmorphogenesis is associated with deregulated expression of known cystogenic molecules, as well as Indian hedgehog. *American Journal of Physiology. Renal Physiology*, *298*, F346–F356.
- Chen, J. K., Taipale, J., Cooper, M. K., & Beachy, P. A. (2002). Inhibition of hedgehog signaling by direct binding of cyclopamine to smoothened. *Genes & Development*, *16*, 2743–2748.
- Chiu, M. G., Johnson, T. M., Woolf, A. S., Dahm-Vicker, E. M., Long, D. A., Guay-Woodford, L., Hillman, K. A., Bawumia, S., Venner, K., Hughes, R. C., Poirier, F., & Winyard, P. J. D. (2006). Galectin-3 associates with the primary cilium and modulates cyst growth in congenital polycystic kidney disease. *The American Journal of Pathology*, *169*, 1925–1938.
- Clearman, K. R., Haycraft, C. J., Croyle, M. J., Collawn, J. F., & Yoder, B. K. (2023). Functions of the primary cilium in the kidney and its connection with renal diseases. *Current Topics in Developmental Biology*, *155*, 39–94.
- Fokkema, I. F., Taschner, P. E., Schaafsma, G. C., Celli, J., Laros, J. F., & den Dunnen, J. T. (2011). LOVD v.2.0: The next generation in gene variant databases. *Human Mutation*, *32*, 557–563.
- Greenberg, D., D’Cruz, R., Lacanlale, J. L., Rowan, C. J., & Rosenblum, N. D. (2023). Hedgehog-Gli mediated control of renal formation and malformation. *Frontiers in Nephrology*, *3*, 1176347.
- Hiratsuka, K., Miyoshi, T., Kroll, K. T., Gupta, N. R., Lewis, J. A., & Morizane, R. (2022). Organoid-on-a-chip model of human ARPKD reveals mechanosensing pathomechanisms for drug discovery. *Science Advances*, *8*, eabq0866.
- Hou, X., Mrug, M., Yoder, B. K., Lefkowitz, E. J., Kremmidiotis, G., D’Eustachio, P., Beier, D. R., & Guay-Woodford, L. M. (2002). Cystin, a novel cilia-associated protein, is disrupted in the cpk mouse model of polycystic kidney disease. *The Journal of Clinical Investigation*, *109*, 533–540.
- Howden, S. E., Wilson, S. B., Groenewegen, E., Starks, L., Forbes, T. A., Tan, K. S., Vanslambrouck, J. M., Holloway, E. M., Chen, Y. H., Jain, S., Spence, J. R., & Little, M. H. (2021). Plasticity of distal nephron epithelia from human kidney organoids enables the induction of ureteric tip and stalk. *Cell Stem Cell*, *28*, 671–684.
- Hsieh, C. L., Jerman, S. J., & Sun, Z. (2022). Non-cell-autonomous activation of hedgehog signaling contributes to disease progression in a mouse model of renal cystic ciliopathy. *Human Molecular Genetics*, *31*, 4228–4240.
- Hu, M. C., Mo, R., Bhella, S., Wilson, C. W., Chuang, P.-T., Hui, C.-C., & Rosenblum, N. D. (2006). GLI3-dependent transcriptional repression of *Gli1*, *Gli2* and kidney patterning genes disrupts renal morphogenesis. *Development*, *133*, 569–578.
- Huang, J. L., Woolf, A. S., Kolatsi-Joannou, M., Baluk, P., Sandford, R. N., Peters, D. J. M., McDonald, D. M., Price, K. L., Winyard, P. J. D., & Long, D. A. (2016). Vascular endothelial growth factor C for polycystic kidney diseases. *Journal of the American Society of Nephrology*, *27*, 69–77.
- Hui, C. C., & Joyner, A. L. (1993). A mouse model of Greig cephalopolysyndactyly syndrome: The *extra-toes1* mutation contains an intragenic deletion of the *Gli3* gene. *Nature Genetics*, *3*, 241–246.
- Ishimoto, Y., Menezes, L. F., Zhou, F., Yoshida, T., Komori, T., Qiu, J., Young, M. F., Lu, H., Potapova, S., Outeda, P., Watnick, T., & Germino, G. G. (2023). A novel ARPKD mouse model with near-complete deletion of the polycystic kidney and hepatic disease 1 (*Pkhd1*) genomic locus presents with multiple phenotypes but not renal cysts. *Kidney International*, *104*, 611–616.

- Johnson, D. R. (1967). Extra-toes: A new mutant gene causing multiple abnormalities in the mouse. *Development*, *17*, 543–581.
- Johnston, J. J., Olivos-Glander, I., Killoran, C., Elson, E., Turner, J. T., Peters, K. F., Abbott, M. H., Aughton, D. J., Aylsworth, A. S., Bamshad, M. J., Booth, C., Curry, C. J., David, A., Dinulos, M. B., Flannery, D. B., Fox, M. A., Graham, J. M., Grange, D. K., Guttmacher, A. E., ... Biesecker, L. G. (2005). Molecular and clinical analyses of Greig Cephalopolysyndactyly and Pallister-hall syndromes: Robust phenotype prediction from the type and position of GLI3 mutations. *The American Journal of Human Genetics*, *76*, 609–622.
- Jonassen, J. A., SanAgustin, J., Baker, S. P., & Pazour, G. J. (2012). Disruption of IFT complex a causes cystic kidneys without mitotic spindle misorientation. *Journal of the American Society of Nephrology*, *23*, 641–651.
- Kakade, V. R., Tao, S., Rajagopal, M., Zhou, X., Li, X., Yu, A. S., Calvet, J. P., Pandey, P., & Rao, R. (2016). A cAMP and CREB-mediated feed-forward mechanism regulates GSK3beta in polycystic kidney disease. *Journal of Molecular Cell Biology*, *8*, 464–476.
- Li, Y., Tian, X., Ma, M., Jerman, S., Kong, S., Somlo, S., & Sun, Z. (2016). Deletion of ADP Ribosylation factor-like GTPase 13B leads to kidney cysts. *Journal of the American Society of Nephrology*, *27*, 3628–3638.
- Low, J. H., Li, P., Chew, E. G. Y., Zhou, B., Suzuki, K., Zhang, T., Lian, M. M., Liu, M., Aizawa, E., Rodriguez Esteban, C., Yong, K. S. M., Chen, Q., Campistol, J. M., Fang, M., Khor, C. C., Foo, J. N., Izpisua Belmonte, J. C., & Xia, Y. (2019). Generation of human PSC-derived kidney organoids with patterned nephron segments and a De novo vascular network. *Cell Stem Cell*, *25*, 373–387.
- Ma, M., Legue, E., Tian, X., Somlo, S., & Liem, K. F., Jr. (2019). Cell-autonomous hedgehog signaling is not required for cyst formation in autosomal dominant polycystic kidney disease. *Journal of the American Society of Nephrology*, *30*, 2103–2111.
- Mandell, J., Koch, W. K., Nidess, R., Preminger, G. M., & McFarland, E. (1983). Congenital polycystic kidney disease. Genetically transmitted infantile polycystic kidney disease in C57BL/6J mice. *American Journal of Pathology*, *113*, 112–114.
- Matissek, S. J., & Elswa, S. F. (2020). GLI3: A mediator of genetic diseases, development and cancer. *Cell Communication and Signaling*, *18*, 54.
- McClelland, K., Li, W., & Rosenblum, N. D. (2022). Pallister-hall syndrome, *GLI3*, and kidney malformation. *American Journal of Medical Genetics Part C: Seminars in Medical Genetics*, *190*, 264–278.
- Mekahli, D., Liebau, M. C., Cadnapaphornchai, M. A., Goldstein, S. L., Greenbaum, L. A., Litwin, M., Seeman, T., Schaefer, F., & Guay-Woodford, L. M. (2023). Design of two ongoing clinical trials of tolvaptan in the treatment of pediatric patients with autosomal recessive polycystic kidney disease. *BMC Nephrology*, *24*, 33.
- Meyers-Needham, M., Lewis, J. A., Gencer, S., Sentelle, R. D., Saddoughi, S. A., Clarke, C. J., Hannun, Y. A., Norell, H., Da Palma, T. M., Nishimura, M., Kravka, J. M., Khavandgar, Z., Murshed, M., Cevik, M. O., & Ogretmen, B. (2012). Off-target function of the sonic hedgehog inhibitor Cyclopamine in mediating apoptosis via nitric oxide-dependent neutral sphingomyelinase 2/ceramide induction. *Molecular Cancer Therapeutics*, *11*, 1092–1102.
- Nakanishi, K., Sweeney, W. E., Zerres, K., Guay-Woodford, L. M., & Avner, E. D. (2000). Proximal tubular cysts in fetal human autosomal recessive polycystic kidney disease. *Journal of the American Society of Nephrology*, *11*, 760–763.
- Papadimitriou, A., Romagnani, P., Angelotti, M. L., Noor, M., Corcoran, J., Raby, K., Wilson, P. D., Li, J., Fraser, D., Piedagnel, R., Hendry, B. M., & Xu, Q. (2020). Collecting duct cells show differential retinoic acid responses to acute versus chronic kidney injury stimuli. *Scientific Reports*, *10*, 16683.
- Prie, D., Friedlander, G., Coureau, C., Vandewalle, A., Cassingena, R., & Ronco, P. M. (1995). Role of adenosine on glucagon-induced cAMP in a human cortical collecting duct cell line. *Kidney International*, *47*, 1310–1318.
- Sato, Y., Yamamura, M., Sasaki, M., & Harada, K. (2018). Blockade of hedgehog signaling attenuates biliary Cystogenesis in the polycystic kidney (PCK) rat. *The American Journal of Pathology*, *188*, 2251–2263.
- Sharma, M., Reif, G. A., & Wallace, D. P. (2019). In vitro cyst formation of ADPKD cells. *Methods in Cell Biology*, *153*, 93–111.
- Silva, L. M., Jacobs, D. T., Allard, B. A., Fields, T. A., Sharma, M., Wallace, D. P., & Tran, P. V. (2018). Inhibition of hedgehog signaling suppresses proliferation and microcyst formation of human autosomal dominant polycystic kidney disease cells. *Scientific Reports*, *8*, 4985.
- Song, X., Di Giovanni, V., He, N., Wang, K., Ingram, A., Rosenblum, N. D., & Pei, Y. (2009). Systems biology of autosomal dominant polycystic kidney disease (ADPKD): Computational identification of gene expression pathways and integrated regulatory networks. *Human Molecular Genetics*, *18*, 2328–2343.
- Tao, S., Kakade, V. R., Woodgett, J. R., Pandey, P., Suderman, E. D., Rajagopal, M., & Rao, R. (2015). Glycogen synthase kinase-3 $\beta$  promotes cyst expansion in polycystic kidney disease. *Kidney International*, *87*, 1164–1175.
- Tran, P. V., Talbott, G. C., Turbe-Doan, A., Jacobs, D. T., Schonfeld, M. P., Silva, L. M., Chatterjee, A., Prysak, M., Allard, B. A., & Beier, D. R. (2014). Downregulating hedgehog signaling reduces renal cystogenic potential of mouse models. *Journal of the American Society of Nephrology*, *25*, 2201–2212.
- Valenti, G., Frigeri, A., Ronco, P. M., D'Ettoire, C., & Svelto, M. (1996). Expression and functional analysis of water channels in a stably AQP2-transfected human collecting duct cell line. *Journal of Biological Chemistry*, *271*, 24365–24370.
- Williams, S. S., Cobo-Stark, P., James, L. R., Somlo, S., & Igarashi, P. (2008). Kidney cysts, pancreatic cysts, and biliary disease in a mouse model of autosomal recessive polycystic kidney disease. *Pediatric Nephrology*, *23*, 733–741.
- Woollard, J. R., Punyashtiti, R., Richardson, S., Masyuk, T. V., Whelan, S., Huang, B. Q., Lager, D. J., vanDeursen, J., Torres, V. E., Gattone, V. H., LaRusso, N. F., Harris, P. C., & Ward, C. J. (2007). A mouse model of autosomal recessive polycystic kidney disease with biliary duct and proximal tubule dilatation. *Kidney International*, *72*, 328–336.
- Yang, C., Harafuji, N., Caldovic, L., Yu, W., Boddu, R., Bhattacharya, S., Barseghyan, H., Gordish-Dressman, H., Foreman, O., Bebok, Z., Eicher, E. M., & Guay-Woodford, L. M. (2023). Pkhd1cyli/cyli mice have altered renal Pkhd1 mRNA processing and hormonally sensitive liver disease. *Journal of Molecular Medicine*, *101*, 1141–1151.
- Ye, H., Wang, X., Constans, M. M., Sussman, C. R., Chebib, F. T., Irazabal, M. V., Young, W. F., Jr., Harris, P. C., Kirschner, L. S., & Torres, V. E. (2017). The regulatory 1alpha subunit of protein kinase a modulates renal cystogenesis.

*American Journal of Physiology. Renal Physiology*, 313, F677–F686.

Zhang, X., Harrington, N., Moraes, R. C., Wu, M.-F., Hilsenbeck, S. G., & Lewis, M. T. (2009). Cyclopamine inhibition of human breast cancer cell growth independent of smoothened (Smo). *Breast Cancer Research and Treatment*, 115, 505–521.

Zhang, Y. J., Yang, C., Wang, W., Harafuji, N., Stasiak, P., Bell, P. D., Caldovic, L., Sztul, E., Guay-Woodford, L. M., & Bebok, Z. (2023). Cystin is required for maintaining fibrocystin (FPC) levels and safeguarding proteome integrity in mouse renal epithelial cells. *The FASEB Journal*, 37, e23008.

**How to cite this article:** Russell, L. G., Kolatsi-Joannou, M., Wilson, L., Chandler, J. C., Tejedor, N. P., Stagg, G., Price, K. L., Rowan, C. J., Crompton, T., Rosenblum, N. D., Winyard, P. J. D., & Long, D. A. (2025). Reduction of elevated *Gli3* does not alter the progression of autosomal recessive polycystic kidney disease. *Physiological Reports*, 13, e70191. <https://doi.org/10.14814/phy2.70191>